

Letter of Intent for J-PARC 50 GeV Proton Synchrotron  
**Search for  $K^-pp$  Bound State**  
**by Stopped  $K^-$  Absorption Reaction on  $^3\text{He}$**

H. Fujioka<sup>a\*</sup> (contact person), R. S. Hayano<sup>b</sup>, T. Hiraiwa<sup>a</sup>, Y. Ishiguro<sup>a</sup>,  
T. Nagae<sup>a</sup>, Y. Sada<sup>a</sup>, T. Suzuki<sup>b</sup>, T. Yamazaki<sup>b,c</sup>

<sup>a</sup> Department of Physics, Kyoto University, Japan

<sup>b</sup> Department of Physics, University of Tokyo, Japan

<sup>c</sup> RIKEN Nishina Center, RIKEN, Japan

December 6, 2010

### Abstract

Stopped  $K^-$  absorption in helium-4 and  $p$ -shell nuclei was investigated in the last decade, and a number of back-to-back  $\Lambda$ - $p$  pairs, not originating from a simple two-nucleon absorption process, were observed. They may be the decay particles of  $K^-pp$  bound states, whose existence are supported by a variety of theoretical calculations.

In order to investigate the existence of  $K^-pp$  bound states, we propose a new measurement of  $K^-$  absorption at rest in helium-3, by using a part of the E15/E17 setup at the K1.8BR beamline.

## 1 Introduction

Akaishi and Yamazaki predicted the existence of  $\bar{K}$ -nuclear bound states, such as  $K^-pp$ ,  $K^-ppn$  and  $K^-ppnn$ , in 2002 [1, 2]. They constructed a phenomenological  $\bar{K}N$  potential, based on the assumption that the  $\Lambda(1405)$  resonance is a  $\bar{K}N$  bound state instead of a normal baryon with three valence quarks, as well as experimental information on antikaon-nucleon scattering and kaonic hydrogen atom. An intriguing conclusion was that the  $K^-ppn$  bound state may have a narrow decay width of 20 MeV because it will lie below the  $\Sigma+\pi$  decay threshold, which forbids the main decay channel energetically. If the width is sufficiently narrow, the experimental observation of such an exotic system may be possible.

---

\*e-mail: fujioka@scphys.kyoto-u.ac.jp

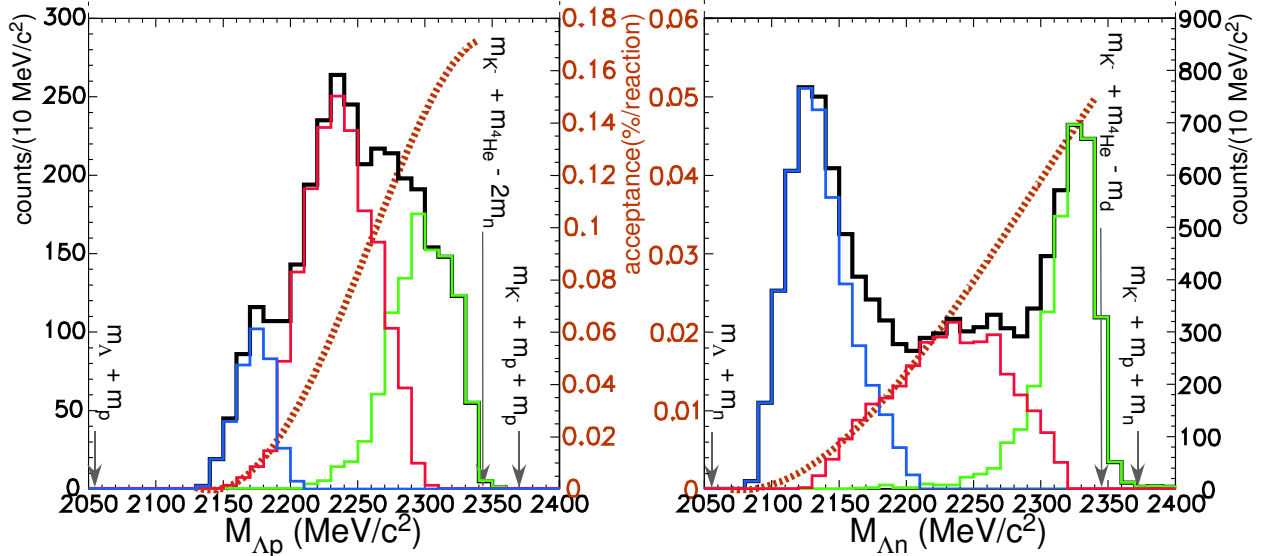
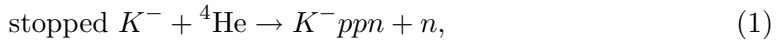


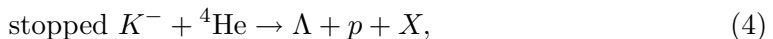
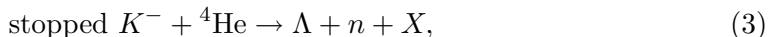
Figure 1: Invariant mass distribution of back-to-back  $\Lambda p$  pair (left) and  $\Lambda n$  pairs. The histograms are divided into three, according to the missing mass (see text for details). The dotted brown curve represents the acceptance function. Taken from Fig. 1 of Ref. [6].

Motivated by their suggestion to utilize the stopped  $K^-$  absorption method [1], experimental studies of the nuclear Auger process for helium-4, *i.e.*,



were carried out by the KEK-PS E471/E549 group. As a result, the existence of a bound state with a very narrow width ( $\lesssim 20$  MeV), which was the original prediction (for  $K^- ppn$ ) by Akaishi and Yamazaki [1], was almost ruled out; a tight upper limit (95% C.L.) of its formation probability of 1% per stopped  $K^-$  at most was obtained for each channel [3, 4]. Still, it is difficult to state only by missing-mass spectroscopy whether a bound state with a rather large width does exist or not.

Furthermore, they also analyzed  $\Lambda N$  pairs in back-to-back, from the following reactions:



where  $X$  denotes missing two nucleons (or a deuteron), plus a  $\gamma$  (in case of a  $\Sigma^0$  in the final state) and possibly a pion [5, 6]. If the final state includes a pion (mesonic absorption), the missing mass ( $m_X$ ) must exceed  $2m_N + m_\pi$ , where  $m_N$  and  $m_\pi$  are the mass of a nucleon and a pion, respectively. On the other hand, when two-nucleon absorption (2NA) takes place, other two spectator nucleons are unobserved and  $m_X$  should be close to  $2m_N$  (or the deuteron mass  $m_d$ ).

Figure 1 shows the invariant mass of observed  $\Lambda N$  pairs. They divided the missing-mass  $m_X$  into three regions, at  $2m_n + 40$  MeV/ $c^2$  and  $2m_n + m_{\pi^0}$  for observed  $\Lambda p$  pairs

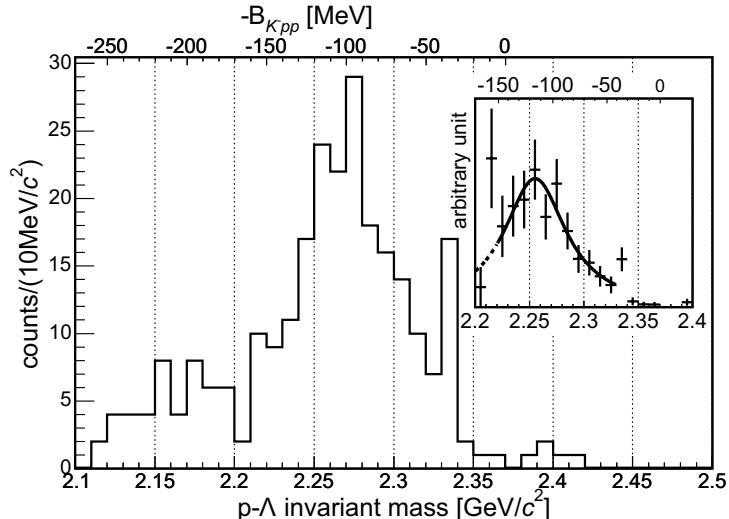


Figure 2: Invariant mass of proton and  $\Lambda$  emitted in the opposite direction ( $\cos\theta < -0.8$ ) from stopped  $K^-$  absorption in  ${}^6/{}^7\text{Li}$  and  ${}^{12}\text{C}$ . Taken from Fig. 3 of Ref. [8].

with  $nn$  or  $(NN\pi)^0$  missing, or at  $m_d + 25 \text{ MeV}/c^2$  and  $m_p + m_n + m_{\pi^0}$  for observed  $\Lambda n$  pairs with  $pn$  (including deuteron) or  $(NN\pi)^+$  missing. The green histogram corresponds to the missing mass in the lowest mass region, indicating the  $\Lambda N$  branch, instead of the  $\Sigma^0 N$  branch, of the 2NA process. The contribution of mesonic absorption can be confined to the blue histogram, with the missing mass in the highest mass region. The remaining component, of which the missing mass is in the middle mass region, is drawn in the red histogram.

The origin of this red component is difficult to explain. One conventional possibility is the contribution of the  $\Sigma N$  branch in the 2NA process, which is followed by  $\Sigma$ - $\Lambda$  conversion or electromagnetic decay of  $\Sigma^0$ , but it may contradict with old experimental data by Katz *et al.* [7], which revealed a much larger fraction of  $\Lambda NNN$  in the final state than that of  $\Sigma^0 NNN$ . Instead, exotic interpretations, which attribute the component to strange tribaryons ( $K^-ppn$  and  $K^-pnn$ ) or strange dibaryons ( $K^-pp$  and  $K^-pn$ ), are also suggested in Refs. [5, 6].

Prior to the analysis for helium-4, the FINUDA collaboration investigated back-to-back  $\Lambda p$  pairs after  $K^-$  absorption in  $p$ -shell nuclei in detail [8]. Figure 2 is the invariant mass distribution for back-to-back  $\Lambda p$  pairs from  ${}^6\text{Li}$ ,  ${}^7\text{Li}$ , and  ${}^{12}\text{C}$ . Again, the contribution of the 2NA process, which should concentrate just below the threshold at  $2m_p + m_{K^-} = 2.370 \text{ GeV}/c^2$ , can not explain the whole spectrum. They are the first to claim an interpretation that the back-to-back  $\Lambda p$  pairs may originate from the decay of a deeply-bound kaonic nuclear state  $K^-pp$ , produced in a kaon absorption process. By fitting the acceptance-corrected spectrum simply with a Lorentzian function, the binding energy and decay width were obtained as  $B = 115_{-5}^{+6+3} \text{ MeV}$  and  $\Gamma = 67_{-11}^{+14+2} \text{ MeV}$ , respectively.

However, this interpretation has been criticized by Magas *et al.* [9] They considered final state interaction (FSI) for  $\Lambda$  and proton from the 2NA process, namely rescattering with a nucleon inside the residue, which loses the kinetic energy of the outgoing particle. Thus, they succeeded in reproducing the invariant mass spectrum of the FINUDA

experiment. On the other hand, secondary rescattering loses the back-to-back angular correlation, which is very strong soon after the 2NA process, and it seems that their result on the opening angle after FSI does not account for the experimental data. It has been also pointed out by Yamazaki and Akaishi [10]. The effect of FSI after the 2NA process was reexamined recently by Pandejee *et al.* [11] using quantum-mechanical scattering theory, and obtained a consistent result with Magas *et al.*'s one. It should be notable that they considered elastic scattering with the residue in analogy with  $(p, p')$  or  $(e, e')$  scattering, which was not taken into account by Magas *et al.*, and that they found its contribution is not visible in the experimental spectrum.

At the moment, the existence of a back-to-back  $\Lambda$ - $p$  pair, which is the product of non-mesonic processes except for a simple 2NA one — hereafter named a *low-mass  $\Lambda$ - $p$  pair* in this LoI, because their invariant mass is much smaller than the expectation when assuming the  $\Lambda p$  branch of the 2NA process — is experimentally robust. Meanwhile, the ambiguity of interpretations on its origin is yet to be settled.

Here, we would like to raise two open questions.

**Question 1** How is the dependence of the target nuclei, in which stopped  $K^-$  is absorbed? Can we see low-mass  $\Lambda$ - $p$  pairs even from helium-3?

Because the 2NA process for deuterium target is kinematically trivial ( $K^- + d \rightarrow \Lambda + n$ ), it is interesting to investigate the  $K^-$  absorption process for helium-3. Needless to say, the effect of FSI is minimized then, compared with the case of helium-4 and heavier nuclei.

**Question 2** How is the correlation among a  $\Lambda$ , a proton, and *each* nucleon in the residue?

A “kinematically complete” measurement of *all* the particles in the final state will provide powerful information on the effect of FSI. An effective way is to decrease the number of participants, such as helium-3, and identify the  $\Lambda pn$  final state. It may be worthwhile to mention that the E549 experiment is analyzing the coincidence of another neutron in addition to the  $\Lambda N$  pair [12].

Therefore, we would like to propose a new experimental program to investigate non-mesonic absorption processes for helium-3:

$$\text{stopped } K^- + {}^3\text{He} \rightarrow \Lambda + p + n, \quad (5)$$

which may include production reactions of  $\overline{K}NN$  bound states:

$$\text{stopped } K^- + {}^3\text{He} \rightarrow K^- pp + n \rightarrow (\Lambda + p) + n, \quad (6)$$

$$\text{stopped } K^- + {}^3\text{He} \rightarrow K^- pn + p \rightarrow (\Lambda + n) + p. \quad (7)$$

If low-mass  $\Lambda$ - $p$  pairs from  ${}^3\text{He}$  are observed experimentally, we will be able to analyze the correlation among the three particles ( $\Lambda$ , proton, and neutron) by use of a Dalitz plot. If the contribution of other processes can be distinguished from that of the production of kaon-bound states, we may be able to extract information on the possible existence of  $K^-pp$  (and  $K^-pn$ ) bound states.

In addition to the FINUDA experiment, the FOPI experiment at GSI (heavy ion collision) [13], the OBELIX experiment at CERN ( $\bar{p}$ - $^4\text{He}$  annihilation) [14], and the DISTO experiment at SATURNE (proton-proton collision) [15] claim the observation of kaon-nuclear bound states, although their existence is not established at present. Further experiments with various kinds of reactions are awaited, as well as the improvement of theoretical understandings about the  $\Lambda(1405)$  and kaon-bound states. For example, two experiments — the E15 experiment with the (in-flight  $K^-$ ,  $n$ ) reaction, and the E27 experiment with the ( $\pi^+$ ,  $K^+$ ) reaction — have been already stage-2 approved at J-PARC. The FOPI experiment [16,17] carried out the proton-proton collision with higher energies than the DISTO experiment. The AMADEUS project [18,19] will investigate kaon-bound states via stopped  $K^-$  absorption in helium-3 and helium-4 at DAΦNE.

The method of stopped  $K^-$  absorption may be complementary to these other reactions, once we have a better understanding of the background, such as two-nucleon absorption processes, which may be followed by FSI.

## 2 Past experiments on $K^-$ absorption at rest

$K^-$ -nuclear absorption at rest had been extensively investigated from the late 1950's till the 1970's, by using emulsions and a variety of bubble chambers, which were filled with hydrogen, deuterium, helium-4, a neon-hydrogen mixture, freon, a freon-propane mixture, and a hydrocarbon mixture. One of the initial attempts was to extract information on the nucleon density at the nuclear surface through the branching ratios of an absorption process of an antikaon in an atomic orbit on a nucleon, mostly at the surface. This process is referred as *one-nucleon absorption*:  $K^- + "N" \rightarrow Y + \pi$ , where " $N$ " denotes a nucleon inside the nucleus, and  $Y$  is a hyperon ( $\Lambda$  or  $\Sigma$ ).

Though it is the most dominant process among all the possible channels, the probability to have no pion in the final state was found to be fairly large. It has to involve two or more nucleons in  $K^-$  absorption (*multi-nucleon absorption*). Its branching ratio is as large as 20% per stopped  $K^-$  for helium-4 and heavier nuclei [20], while it is only  $\sim 1\%$  for deuterium [21].

A detailed analysis with a helium-4 bubble chamber was performed by Katz *et al.* [7] For example, the branching ratios into  $(\Lambda \text{ or } \Sigma^0)(pnn)^1$ ,  $\Sigma^+nnn$ ,  $\Sigma^-pd$ , and  $\Sigma^-ppn$  were given as  $11.7 \pm 2.4\%$ ,  $1.0 \pm 0.4\%$ ,  $1.6 \pm 0.6\%$ , and  $2.0 \pm 0.7\%$  per stopped  $K^-$ , respectively. Assuming the isospin symmetry among  $\Sigma$ 's, the first one can be decomposed into  $9.4 \pm 2.6\%$  for  $\Lambda(ppn)$  and  $2.3 \pm 1.0\%$  for  $\Sigma^0(ppn)$ . The multi-nucleon absorption process accounts for  $16.4 \pm 2.6\%$  in total.

By the way, it is known that three kinds of secondary processes have to be taken into account, at least for one-nucleon absorption processes: i)  $\Sigma$ - $\Lambda$  conversion and ii)  $\pi$  reabsorption [22,23], iii) hyperon trapping.

Roughly speaking, about half of  $\Sigma$ 's produced via an one-nucleon absorption process, for helium-4 [7,22] and carbon [23], undergo  $\Sigma$ - $\Lambda$  conversion with a nucleon in the residual nucleus ( $\Sigma N \rightarrow \Lambda N$ ). It was studied through the momentum distribution of pions associated with hyperons. Unfortunately it is not well-known whether this is also important in multi-nucleon absorption processes.

---

<sup>1</sup>"(pnn)" represents that the three nucleons can be bound or unbound, *i.e.*  $p + n + n$  or  $n + d$  or  $t$ .

Conversely, a pion in association with a hyperon can be reabsorbed by the residue. In case of carbon, Vander Velde-Wilquet *et al.* estimated its fraction to be around 0.1–0.2, depending on the charge of the pion and the associated hyperon [20, 23]. Because the final state after this  $\pi$  reabsorption is similar to that from a multi-nucleon absorption process, its contamination should be subtracted from the multi-nucleon absorption rate. Moulder *et al.* reported the observation of a  $\Sigma^-$  with two prongs but without a pion, which may be attributed to a one-nucleon absorption process  $K^- + “p” \rightarrow \Sigma^- + \pi^+$ , followed by  $\pi^+$  reabsorption  $\pi^+ + “pn” \rightarrow p + p$  [24].

In addition, some of  $\Lambda$  hyperons produced in one-nucleon absorption can be trapped to form hyperfragments. They can be easily distinguished from other absorption processes because they decay via weak interaction, and this process will not be discussed anymore in this LoI.

### 3 Possible backgrounds

Based on a collection of the results of old experiments, together with recent FINUDA and KEK-PS E549 experiments, we can list possible  $K^-$ - ${}^3\text{He}$  absorption processes, which yield the  $\Lambda pn$  final state. As discussed above, a primary process (one-nucleon absorption or multi-nucleon absorption) may be followed by a secondary one to some extent.

The primary process of particular importance is two-nucleon absorption (**2NA**). The  $\Lambda pn$  final state can be directly caused by the following  $\Lambda N$  branches of 2NA processes:

$$\text{stopped } K^- + {}^3\text{He} \rightarrow \Lambda + p + n_s, \quad (8)$$

$$\text{stopped } K^- + {}^3\text{He} \rightarrow \Lambda + n + p_s, \quad (9)$$

where the subscript  $s$  stands for the spectator nucleon. The product of a 2NA process, either a hyperon and a nucleon, may be rescattered by the spectator nucleon (**2NA+Rescat.**), like the arguments by Magas *et al.* [9] and Pandejee *et al.* [11]. Moreover, other branches of  $\Sigma^0 N$ ,  $\Sigma^+ n$ , and  $\Sigma^- p$  are also possible, but need to be followed by a  $\Sigma$ - $\Lambda$  conversion process (**2NA+Conv.**), in order to make the final state  $\Lambda pn$ .

Another possible branch of non-mesonic absorption is three-nucleon absorption (**3NA**):

$$\text{stopped } K^- + {}^3\text{He} \rightarrow \Lambda + p + n, \quad (10)$$

in which all the three nucleons are directly involved in the absorption process. In this LoI, the two-step processes of 2NA+Rescat. and 2NA+Conv., which hold a strong correlation among three particles in the final state, as demonstrated later, are strictly discriminated from this *genuine* 3NA process. It is not understood whether the genuine 3NA process does occur.

Last but not least, pion reabsorption after one-nucleon absorption (**1NA+ $\pi$ -Reabs.**) may be seen as the  $\Lambda pn$  final state, which has been already discussed in the previous section. Its contribution should be subtracted in estimating the non-mesonic absorption ratio (for example, see the discussion in Ref. [25]).

In the next section, these background processes are taken into account in a GEANT4-based Monte Carlo simulation, as well as the  $\bar{K} NN$  production reactions.

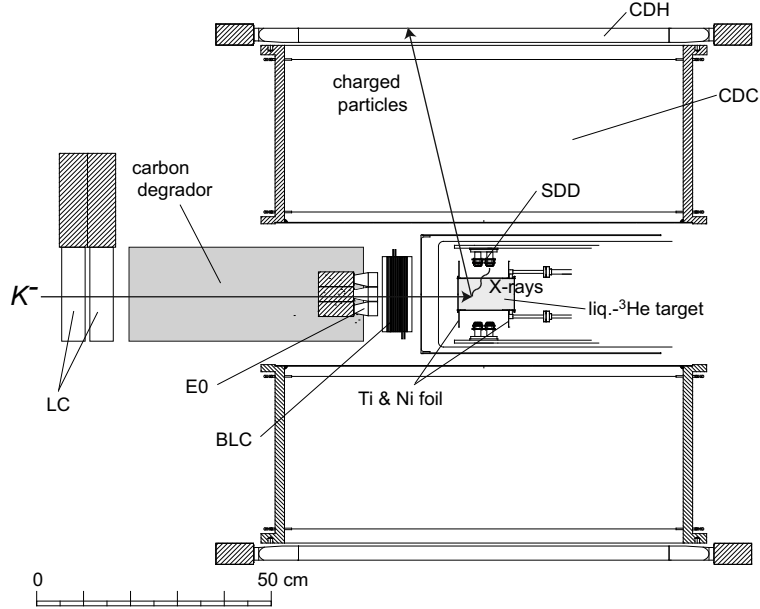


Figure 3: Schematic view of the E17 experimental setup.

## 4 Experimental procedure

### 4.1 Setup

The experiment will be carried out at K1.8BR beamline, where two experiments (E15 and E17) have been already stage-2 approved. It has some features in common with each experiment, as follows:

- stopped  $K^-$  in helium-3 target — The E17 experiment will also stop  $K^-$ 's in the same target so as to form kaonic helium-3 atoms, whose  $3d \rightarrow 2p$  transition X-rays will be measured by silicon drift detectors (SDD).
- measurement of a  $\Lambda$  and a proton — The E15 experiment will investigate *in-flight*  $K^-$  interaction with helium-3 to produce a  $K^-pp$  bound state, whose decay products, a  $\Lambda$  and a proton, will be momentum-analyzed by a cylindrical detector system (CDS).

Therefore, the experimental setup will be practically the same as that of the E17 experiment (Fig. 3), except for the removal of the SDDs and the excitation of the solenoid magnet in the CDS. The K1.8BR beamline, together with the degrader and the subsequent beam defining counter (E0) and the drift chamber (BLC), can be used without any modification.

Two of the three particles in the  $\Lambda pn$  final state, a  $\Lambda$  and a proton, will be directly detected by the CDS with the magnetic field of 0.5 Tesla (nominal) or 0.7 Tesla (maximal). It includes the cylindrical drift chamber (CDC) and the cylindrical detector hodoscopes (CDH) inside the solenoid magnet. It can be used as it is.

In this experiment, the direct detection of the neutron by the neutron counter in the E15 setup is not mandatory. It is because the momentum of a neutron from the  $K^-pp$  production reaction is expected to be around  $400 \text{ MeV}/c$ , much smaller than

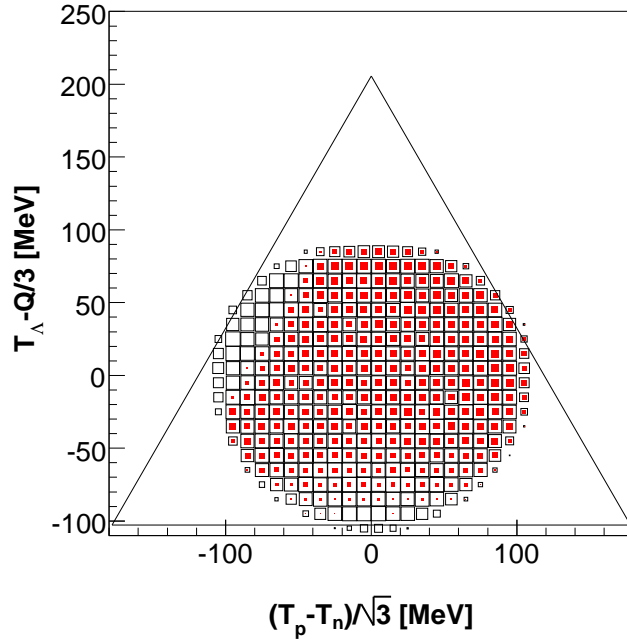


Figure 4: Dalitz plot for the stopped  $K^- + {}^3\text{He} \rightarrow \Lambda + p + n$  reaction ( $Q = 308$  MeV). The region with open boxes corresponds to the kinematically allowed region, and the red filled box represents the acceptance of the  $\Lambda p$  detection by the CDS.

that from the in-flight reaction around  $1300$  MeV/ $c$ , and the identification of the final state, whose detail will be described later, is clear enough even without the detection of this neutron. Needless to say, the utilization of such a counter will bring further interesting outcomes, at the expense of the statistics due to a small solid angle of its coverage.

## 4.2 Dalitz plot analysis

In particle physics, three-body decay of an unstable particle is analyzed by using the Dalitz plot. This technique can be applied in describing kinematical correlation of the  $\Lambda pn$  final state from stopped  $K^-$  absorption in helium-3. While two-nucleon absorption for helium-4 into a specific final state of  $\Lambda dn$  was analyzed in a similar manner [26], this experiment aims to investigate a ‘general’ final state of  $\Lambda pn$  from non-mesonic absorption<sup>2</sup>.

Figure 4 shows a Dalitz plot for this channel. Since there are only two free parameters in describing a three-body final state by constraining the energy-momentum conservation law, an event can be depicted by a point in the Dalitz plot. In this triangle representation, the distance between the point and each side represents the kinetic

<sup>2</sup>An exception is the two-body final state of  $\Lambda d$ . The identification of this branch is beyond the scope of this LoI.

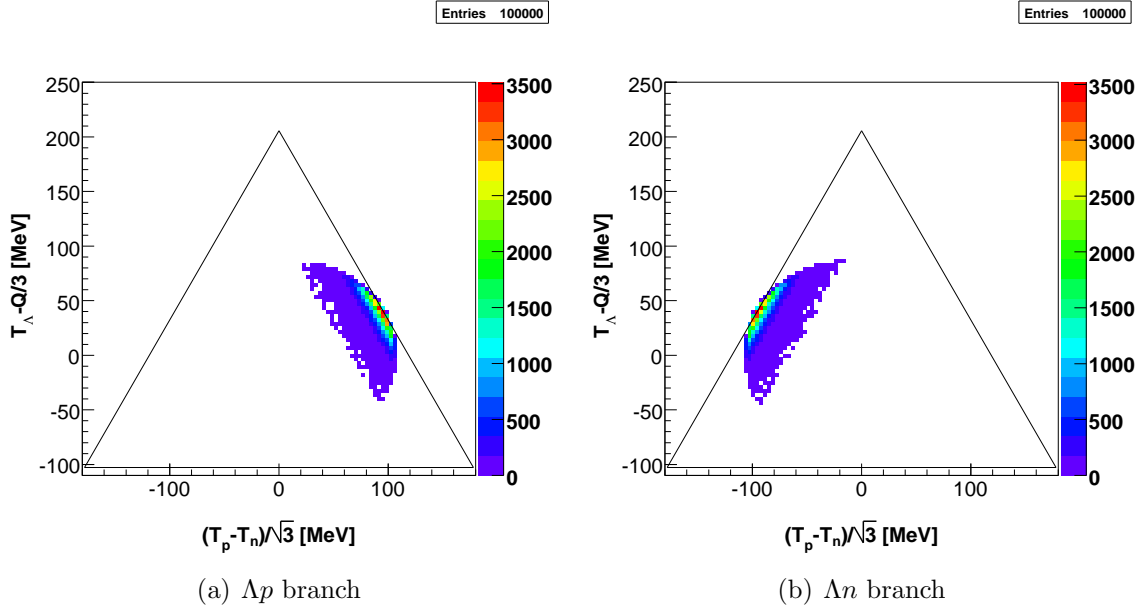


Figure 5: Generated Dalitz plot distributions for 2NA processes in Monte Carlo simulation.

energy of a particle. The capability of the detection of a  $\Lambda$ - $p$  pair in the phase space is estimated by a GEANT4-based Monte Carlo simulation, and reconstructed events are overlaid by red filled boxes in Fig. 4. It is clear that almost all the phase space, except for the upper left and the lower part, can be examined by use of the CDS. The deficit of these two parts is because of the lower detection efficiency of a slow proton and a slow  $\Lambda$ , decaying into a slow proton and a  $\pi^-$ , respectively. As shown later,  $\bar{K}NN$  production events are expected to distribute near the center, where the CDS has an acceptance large enough.

As an example, events of 2NA processes (8) and (9), generated by a Monte Carlo simulation, are displayed in Fig. 5. By comparison with Fig. 4, one can see the  $\Lambda p$  branch can be observed by the CDS, while we have almost no sensitivity of the direct observation of the  $\Lambda n$  branch without any secondary process such as rescattering.

In the simulation, the momentum  $q$  of the spectator nucleon is assumed to follow the distribution:

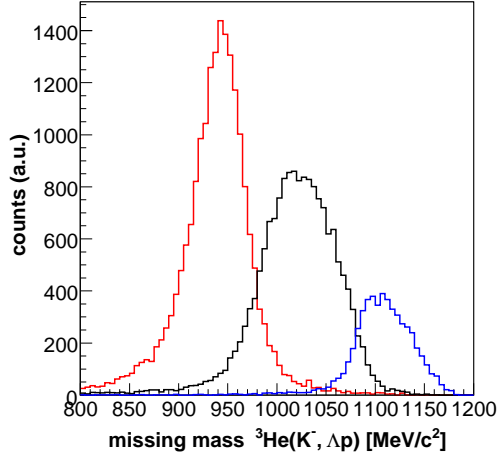
$$\frac{dN}{dq} \propto q^2 \exp\left(-\frac{q^2}{q_0^2}\right), \quad (11)$$

with  $q_0 = 96(\pm 3) \text{ MeV}/c$ , which was obtained by Gotta *et al.* from a similar measurement of a 2NA process for stopped  $\pi^-$  absorption in helium-3 [27]. Because non-mesonic absorption itself is more or less similar except for the difference of absorbed mesons, their analysis would be of some help to foresee the result for stopped  $K^-$  absorption.

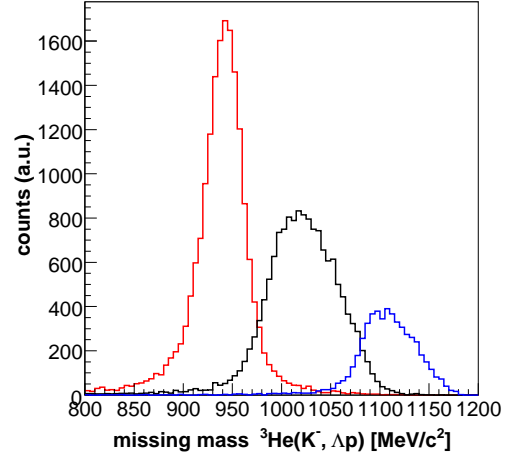
### 4.3 Stopped $\pi^-$ absorption in ${}^3\text{He}$

At PSI, Gotta *et al.* investigated negative pion absorption at rest in helium-3, which resulted in the  $pnn$  (and  $dn$ ) final states [27]. They considered four channels into the  $pnn$  final state: absorption by isoscalar/isotriplet  $NN$  pairs (2NA), two-nucleon emission followed by final state interaction (FSI), and three-nucleon absorption (3NA).





(a)  $B = 0.5$  Tesla



(b)  $B = 0.7$  Tesla

Figure 7: Missing mass distribution for the  $\Lambda p n$  (red),  $\Sigma^0 p n$  (black), and  $\Lambda p N \pi$  (blue) final states. The weight of each channel is arbitrary.

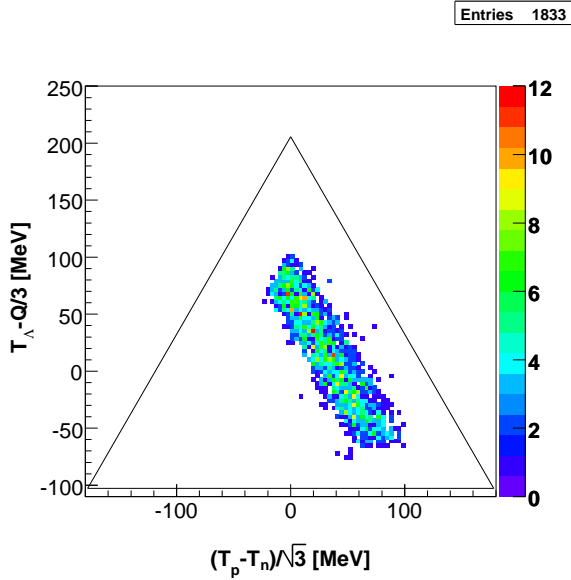


Figure 8: Reconstructed Dalitz plot for the production of  $K^- pp$  bound states with the binding energy fixed to be 100 MeV.

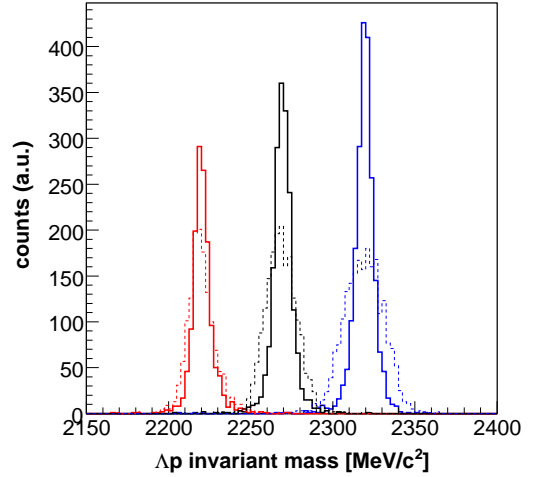


Figure 9: Invariant mass of  $\Lambda$ - $p$  pairs from  $K^- pp$  bound states with the binding energy 150 (red), 100 (black), and 50 MeV (blue). The solid (dashed) histogram correspond to the analysis with (without) the kinematic fitting.

to distinguish the  $\Lambda pn$  final state from the  $\Sigma^0 pn$  one.

In case of the  $\Lambda pn$  final state, the missing mass of the  ${}^3\text{He}(K^-, \Lambda p)X$  reaction should be close to the neutron mass, whereas the  $\Sigma^0 pn$  final state would bring a larger missing mass because of the undetected  $\gamma$  from  $\Sigma^0$  decay. A simulated missing-mass distribution for phase-space distributed  $\Lambda pn$ ,  $\Sigma^0 pn$ , and  $\Lambda p N \pi$  (mesonic final state) events is shown in Fig. 7 for two setting of the magnetic field in the solenoid magnet. It can be seen the separation among the three channels is good enough with the nominal magnetic field (0.5 Tesla), but may be improved slightly by strengthening the field to 0.7 Tesla. In the following simulation, the magnetic field is fixed to be 0.7 Tesla, and the events between 910 and 970 MeV/ $c^2$  are selected.

#### 4.5 Signal: $\bar{K}NN$ production

For simplicity, we consider only the reaction (6), *i.e.* the production of  $K^-pp$  bound states. Figure 8 is a Dalitz plot obtained from the reconstructed  $\Lambda$ - $p$  pairs from  $K^-pp$  decay, where the mass of  $K^-pp$  is fixed to be 2270 MeV/ $c^2$ , corresponding to the binding energy of 100 MeV. Because the emitted neutron is monochromatic, the distribution in the Dalitz plot is parallel to the right oblique line of the triangle.

The invariant mass distribution of reconstructed  $\Lambda$ - $p$  pairs, with three sets of input masses (2220, 2270, and 2320 MeV/ $c^2$ ), is shown in Fig. 9. The resolution is almost constant around 12 MeV/ $c^2$  in FWHM after the kinematic fitting.

#### 4.6 Background: rescattering and $\Sigma$ - $\Lambda$ conversion

The signal will not overlap with the background 2NA process (see Fig. 5), unless the binding energy of  $K^-pp$  states is close to zero. Hence, the secondary process after the 2NA process may be a serious background rather than the 2NA process itself.

For example, the  $\Lambda p$  branch of the 2NA process (reaction (8)) may be followed by rescattering:  $p + n_s \rightarrow p' + n'$  or  $\Lambda + n_s \rightarrow \Lambda' + n'$ . In the former (latter) case, the kinetic energy of the remaining  $\Lambda$  (proton) is unchanged. Therefore, the reconstructed Dalitz plot for the former case (Fig. 10) has a linear locus parallel to the bottom line. Similar structures, parallel to one of three sides of the triangle, can be expected for other type of the 2NA+Rescat. process, as well.

The situation is not largely different for  $\Sigma$ - $\Lambda$  conversion, which can be regarded as inelastic scattering in a sense. Figure 11 is an example of the Dalitz plot, exhibiting the  $\Sigma^-p$  branch of the 2NA process, followed by  $\Sigma^- + p_s \rightarrow \Lambda' + n'$  conversion. Again, other branches with  $\Sigma$ - $\Lambda$  conversion will cause analogous patterns.

In other words, if a Dalitz plot includes such a locus parallel to some line of the triangle, it indicates the effect of a secondary process after the 2NA process, or the  $\bar{K}NN$  production reactions. Seemingly, any linear structure tailed from the 2NA area does not appear in the Dalitz plot of Gotta *et al.* [27]

Besides, one-nucleon absorption followed by pion reabsorption may contribute. As shown in Fig. 12, the kinetic energy of a  $\Lambda$ , which will remain unchanged by the reabsorption, is rather small. Even if it exists to a certain extent, its contribution may be controlled by applying a cut on  $\Lambda$ 's kinetic energy.

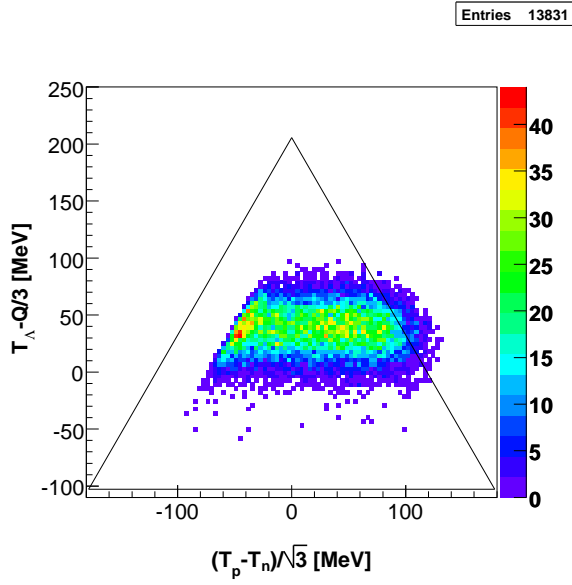


Figure 10: Reconstructed Dalitz plot for the  $\Lambda p$  branch of the 2NA process, followed by  $p$ - $n$  rescattering.

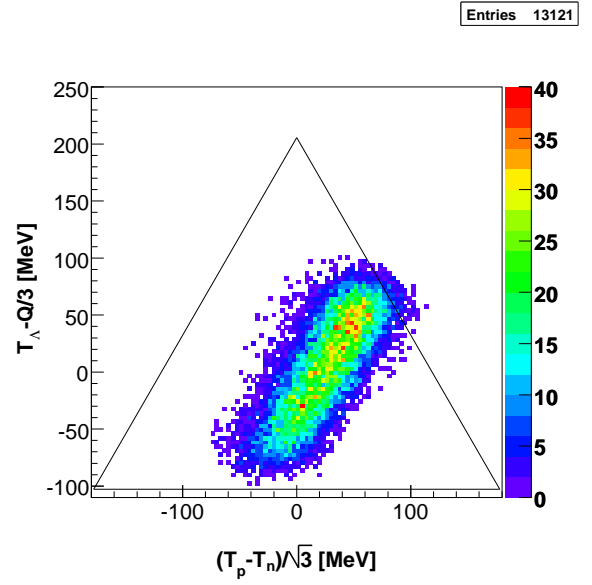


Figure 11: Reconstructed Dalitz plot for the  $\Sigma^- p$  branch of the 2NA process, followed by  $\Sigma^- + p_s \rightarrow \Lambda' + n'$  conversion.

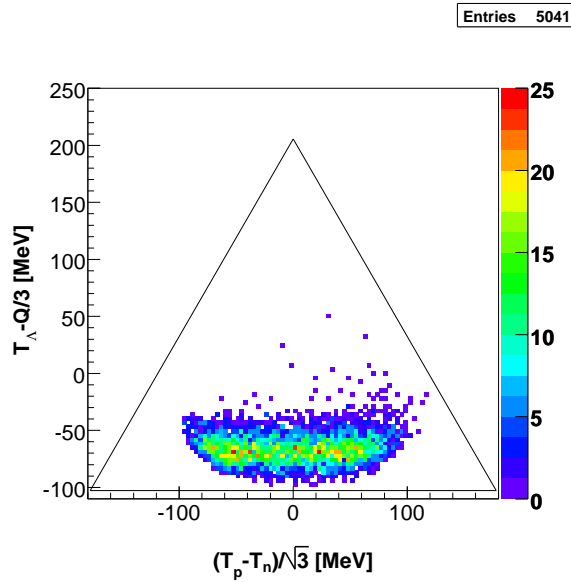


Figure 12: Reconstructed Dalitz plot for an one-nucleon absorption process, followed by  $\pi$  reabsorption.

## 5 Summary

A new experiment to investigate stopped  $K^-$  absorption processes in  ${}^3\text{He}$ , especially the non-mesonic one into the  $\Lambda pn$  final state, is proposed. It may include the production of  $K^-pp$  bound states, as well as the two-nucleon absorption process, sometimes followed by a secondary process such as rescattering or  $\Sigma$ - $\Lambda$  conversion. Compared with past experiments, the advantage of using helium-3 is the capability of a visible separation of each contribution by performing the Dalitz plot analysis with detection of  $\Lambda$ - $p$  pairs.

## References

- [1] Y. Akaishi and T. Yamazaki, Phys. Rev. C **65**, 044005 (2002).
- [2] T. Yamazaki and Y. Akaishi, Phys. Lett. **B515**, 70 (2002).
- [3] M. Sato *et al.*, Phys. Lett. **B659**, 107 (2008).
- [4] H. Yim *et al.*, Phys. Lett. **B688**, 43 (2010).
- [5] T. Suzuki *et al.*, arXiv:0711.4943 [nucl-ex].
- [6] T. Suzuki *et al.*, Mod. Phys. Lett. A **23**, 2520 (2008).
- [7] P. A. Katz *et al.*, Phys. Rev. D **1**, 1267 (1970).
- [8] M. Agnello *et al.*, Phys. Rev. Lett. **94**, 212303 (2005).
- [9] V. K. Magas, E. Oset, A. Ramos, H. Toki, Phys. Rev. C **74**, 025206 (2006).
- [10] T. Yamazaki and Y. Akaishi, Nucl. Phys. **A792**, 229 (2007).
- [11] Grishma Mehta Pandejee, N. J. Upadhyay, and B. K. Jain, Phys. Rev. C **82**, 034608 (2010).
- [12] T. Suzuki, talk at MENU2010 (Jefferson Lab); T. Suzuki, talk at MESON2010 (Jagiellonian University).
- [13] N. Herrmann, in: A. Hirtl. (Eds.), Proceedings of EXA05, Austrian Academy of Science Press., Vienna, 2005, pp. 73–81.
- [14] G. Bendiscioli *et al.*, Nucl. Phys. **A789**, 222 (2007).
- [15] T. Yamazaki *et al.*, Phys. Rev. Lett. **104**, 132502 (2010).
- [16] FOPI Collaboration, Experimental proposal to GSI (2007).
- [17] K. Suzuki *et al.*, Nucl. Phys. **A827**, 312c (2009).
- [18] AMADEUS Collaboration, Letter of Intent (2006).
- [19] J. Zmeskal *et al.*, Nuclear Physics **A835**, 410 (2010).
- [20] C. Vander Velde-Wilquet *et al.*, Nuovo Cimento A **39**, 538 (1977), and references therein.
- [21] V. R. Veirs, R. A. Burnstein, Phys. Rev. D **1**, 1883 (1970).
- [22] E. H. S. Burhop, Nucl. Phys. **B44**, 445 (1972).
- [23] C. Vander Velde-Wilquet *et al.*, Nuovo Cimento A **38**, 178 (1977).
- [24] J. W. Moulder *et al.*, Nucl. Phys. **B35**, 332 (1971).

- [25] H. Davis *et al.*, Nuovo Cimento A**53**, 313 (1968).
- [26] R. Roosen and J. H. Wickens, Nuovo Cimento A **66**, 101 (1981).
- [27] D. Gotta *et al.*, Phys. Rev. C **51**, 469 (1995).